Light as a biomarker:

Computer-assisted reconstruction and analysis of genetic properties of cells from their microscopic images

Eugene Kashdan,
University College Dublin, Ireland

8 June, 2015

Problem statement

Motivation

- In-vitro fertilization (IVF) is a major treatment for infertility when other methods of assisted reproductive technology have failed.

Motivation

- In-vitro fertilization (IVF) is a major treatment for infertility when other methods of assisted reproductive technology have failed.
- The first successful tube-baby was born in the UK in 1978. However, despite its wide use in modern society, the rates of success of IVF treatment are abysmal even in the most developed countries.

Motivation

- In-vitro fertilization (IVF) is a major treatment for infertility when other methods of assisted reproductive technology have failed.
- The first successful tube-baby was born in the UK in 1978. However, despite its wide use in modern society, the rates of success of IVF treatment are abysmal even in the most developed countries.
- Review by the European Society of Human Reproduction and Embryology (2010):

Motivation

- In-vitro fertilization (IVF) is a major treatment for infertility when other methods of assisted reproductive technology have failed.
- The first successful tube-baby was born in the UK in 1978. However, despite its wide use in modern society, the rates of success of IVF treatment are abysmal even in the most developed countries.
- Review by the European Society of Human Reproduction and Embryology (2010): The main issue that needs to be urgently addressed in order to improve the overall IVF success is embryo quality evaluation.

Motivation

- In-vitro fertilization (IVF) is a major treatment for infertility when other methods of assisted reproductive technology have failed.
- The first successful tube-baby was born in the UK in 1978. However, despite its wide use in modern society, the rates of success of IVF treatment are abysmal even in the most developed countries.
- Review by the European Society of Human Reproduction and Embryology (2010): The main issue that needs to be urgently addressed in order to improve the overall IVF success is embryo quality evaluation.
- Current embryo viability evaluation methods depend on the embryologist personal experience and could be qualified more as **art** rather than **science**.

Embryo viability analysis

Human embryo is a thick (up to $100\mu m$ in diameter) almost transparent cell. It cannot be stained or damaged, which limits its observation to specific microscopic modalities and also to the short observation time.

Embryo viability analysis

Human embryo is a thick (up to $100\mu m$ in diameter) almost transparent cell. It cannot be stained or damaged, which limits its observation to specific microscopic modalities and also to the short observation time.

The Differential Interference Contrast (DIC) microscope is commonly used in fertility clinics and the Hoffmann Modulation Contrast (HMC) microscope is employed to lesser degree.

Embryo viability analysis

Human embryo is a thick (up to $100\mu m$ in diameter) almost transparent cell. It cannot be stained or damaged, which limits its observation to specific microscopic modalities and also to the short observation time.

The Differential Interference Contrast (DIC) microscope is commonly used in fertility clinics and the Hoffmann Modulation Contrast (HMC) microscope is employed to lesser degree.

Following a very short (1-2 min.) daily observation, the embryologists examine the shape and the symmetry of the distribution of blastomeres (cells composing the embryos).

Embryo viability analysis

Human embryo is a thick (up to $100\mu m$ in diameter) almost transparent cell. It cannot be stained or damaged, which limits its observation to specific microscopic modalities and also to the short observation time.

The Differential Interference Contrast (DIC) microscope is commonly used in fertility clinics and the Hoffmann Modulation Contrast (HMC) microscope is employed to lesser degree.

Following a very short (1-2 min.) daily observation, the embryologists examine the shape and the symmetry of the distribution of blastomeres (cells composing the embryos).

Based on the impression from the number of two-dimensional images, the embryos are scored, with the highest score reflecting the potential of the embryo to successfully implant within the uterine cavity.

Some technical details

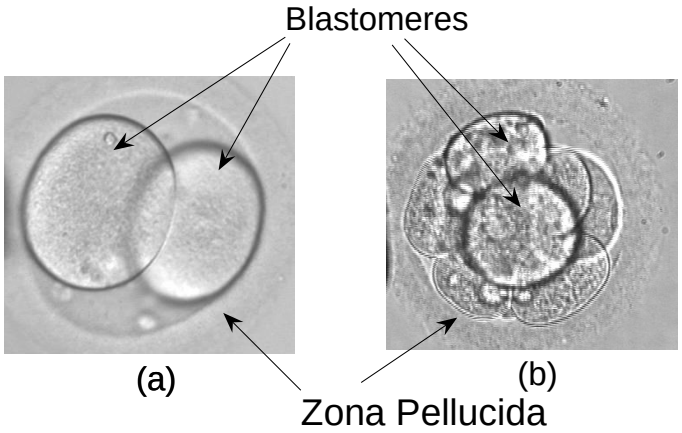

(a) two-blastomere human embryo, (b) eight-blastomere human embryo

- The image has a *relief-like* quality, exhibiting a shadow-cast effect.
- The shadows and highlights indicate the sign and the slope of phase gradient.
- The direction of shadow casting reverses for structures with refractive indices that are lower and higher than the surrounding medium

Some technical details

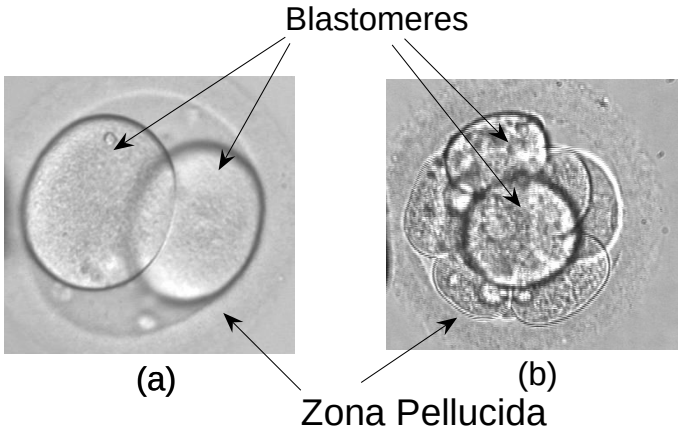

(a) two-blastomere human embryo, (b) eight-blastomere human embryo

- The image has a *relief-like* quality, exhibiting a shadow-cast effect.
- The shadows and highlights indicate the sign and the slope of phase gradient.
- The direction of shadow casting reverses for structures with refractive indices that are lower and higher than the surrounding medium

Some technical details

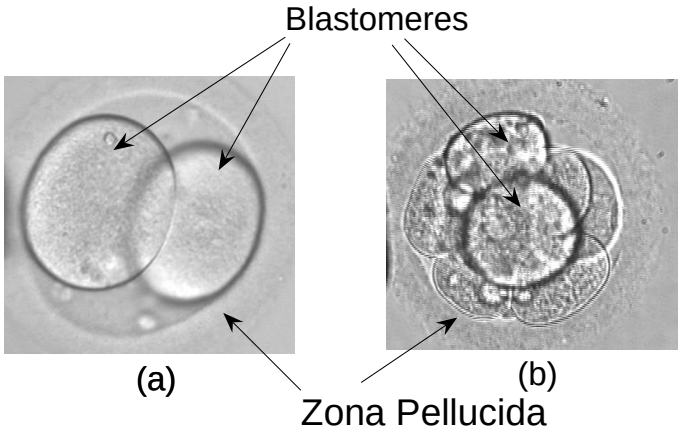

(a) two-blastomere human embryo, (b) eight-blastomere human embryo

- The image has a *relief-like* quality, exhibiting a shadow-cast effect.
- The shadows and highlights indicate the sign and the slope of phase gradient.
- The direction of shadow casting reverses for structures with refractive indices that are lower and higher than the surrounding medium

Caenorhabditis elegans

C. elegans are transparent nematodes used as a model for research in genomics, cell biology, neuroscience and aging.

C. elegans have short life cycle, compact genome and stereotypical development.

C. Elegans embryos

All of C. elegans embryogenesis occurs within a transparent eggshell.

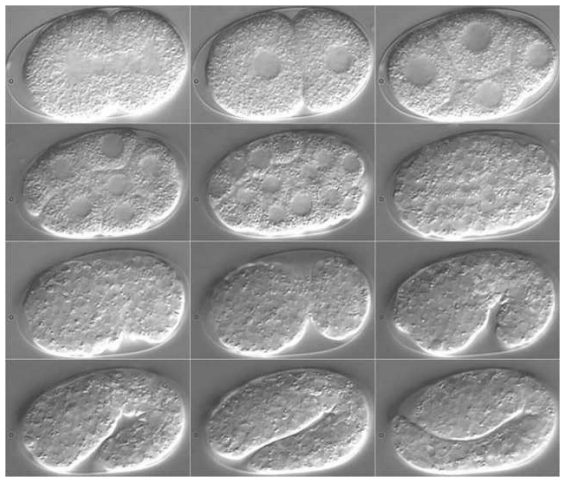

DIC image of the C. elegans embryo at various stages of development

C. Elegans embryos

All of C. elegans embryogenesis occurs within a transparent eggshell.

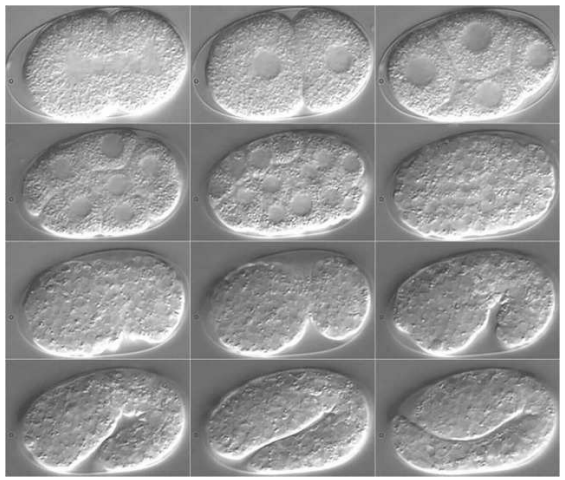

DIC image of the C. elegans embryo at various stages of development

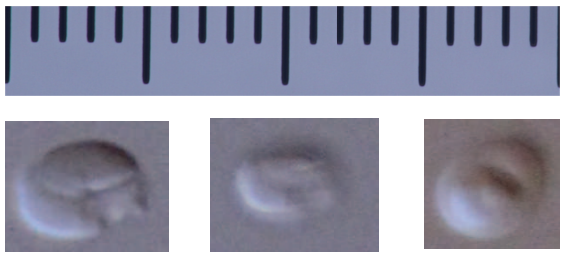

The egg measures about $50\mu m$ in length and $30\mu m$ in width

Mathematics meets genetics

Algorithm

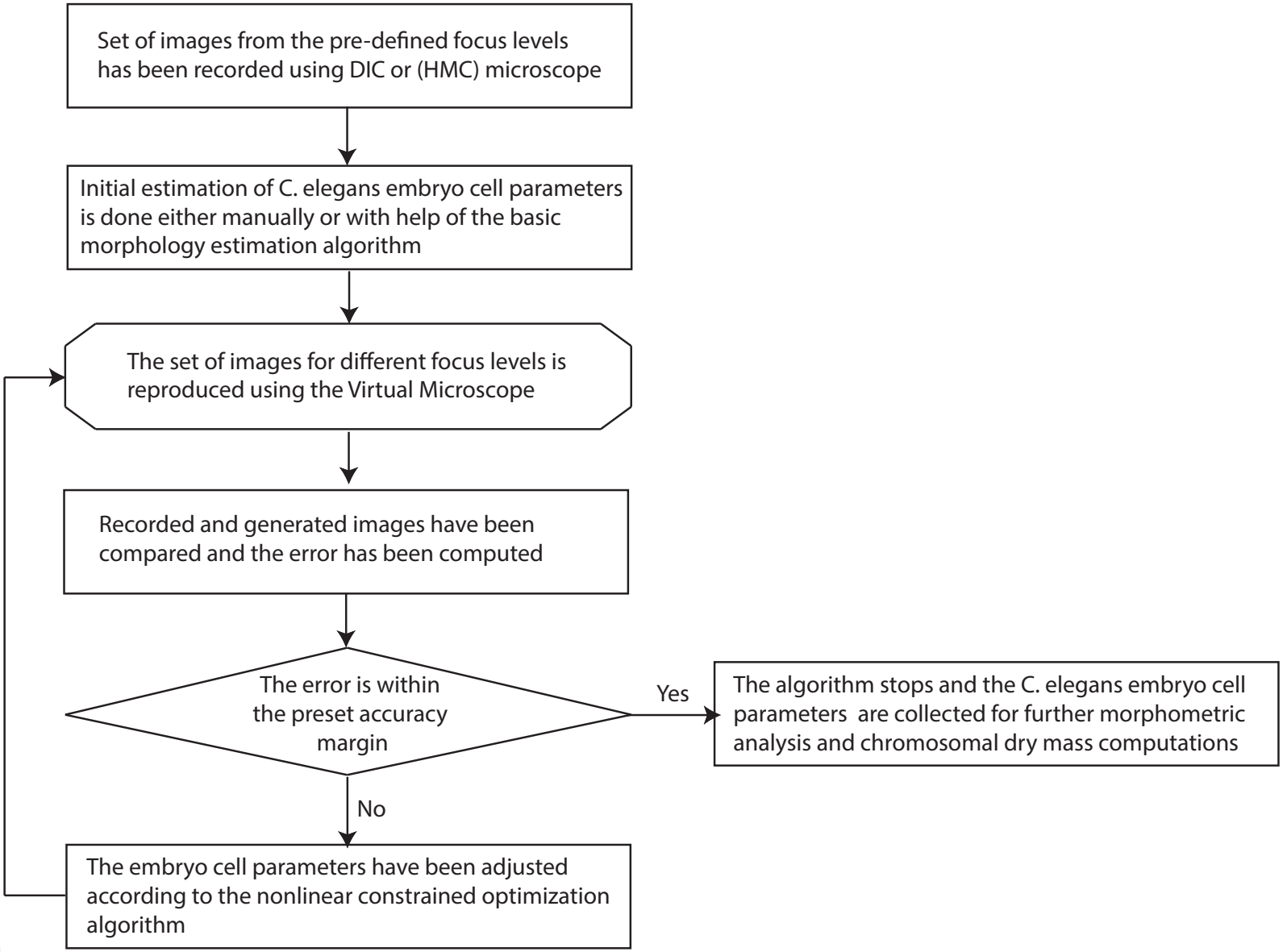

Properties of refractive index

- The refractive index is proportional to the concentration of organic molecules.

Properties of refractive index

- The refractive index is proportional to the concentration of organic molecules.
- It can be used to quantify the aggregation and the surface coverage of cellular proteins and the growth and architectural changes in cells.

Properties of refractive index

- The refractive index is proportional to the concentration of organic molecules.
- It can be used to quantify the aggregation and the surface coverage of cellular proteins and the growth and architectural changes in cells.
- Conventional assertion: rapid cell division and proliferation activity of cancer cells lead to high concentration of protein molecules within cellular organelles and result in the increase of cell refractive index.

Properties of refractive index

- The refractive index is proportional to the concentration of organic molecules.
- It can be used to quantify the aggregation and the surface coverage of cellular proteins and the growth and architectural changes in cells.
- Conventional assertion: rapid cell division and proliferation activity of cancer cells lead to high concentration of protein molecules within cellular organelles and result in the increase of cell refractive index.
- Information about the aneuploidy (missing or additional chromosomes) could be extracted from the refractive index distribution. It is a $\#1$ reason behind the failure of the IVF procedure. Aneuploidy is also a major hallmark of cancer!

Properties of refractive index

- The refractive index is proportional to the concentration of organic molecules.
- It can be used to quantify the aggregation and the surface coverage of cellular proteins and the growth and architectural changes in cells.
- Conventional assertion: rapid cell division and proliferation activity of cancer cells lead to high concentration of protein molecules within cellular organelles and result in the increase of cell refractive index.
- Information about the aneuploidy (missing or additional chromosomes) could be extracted from the refractive index distribution. It is a $\#1$ reason behind the failure of the IVF procedure. Aneuploidy is also a major hallmark of cancer!
- Experimental confirmation for cancer cells: Tomographic Phase Microscope (*X-rays*), Optical Coherence Microscope (*Infrared*).

Reconstruction of genetic properties

The total chromosomal dry mass:

$$m_{chromosome} = \frac{1}{\alpha} \iiint_{V_c} [n(x, y, z) - n_{medium}] dV,$$

where $n(x, y, z)$ and n_{medium} are the refractive index of the chromosome and the culture medium; V_c is the chromosome region; α is the increase in the refractive index value per unit increase in the concentration of the constituent molecules.

Reconstruction of genetic properties

The total chromosomal dry mass:

$$m_{chromosome} = \frac{1}{\alpha} \iiint_{V_c} [n(x, y, z) - n_{medium}] dV,$$

where $n(x, y, z)$ and n_{medium} are the refractive index of the chromosome and the culture medium; V_c is the chromosome region; α is the increase in the refractive index value per unit increase in the concentration of the constituent molecules.

Refractive index distribution $n_{cell}(x, y)$ at transverse position (x, y):

$$n_{cell}(x, y) = \frac{\lambda_0}{4\pi} \frac{\Delta\varphi(x, y)}{t(x, y)} + n_{medium}(x, y).$$

Here λ_0 is a center wavelength in free space, $\Delta\varphi(x, y)$ is a phase map and $t(x, y)$ is a physical thickness of cell at position (x, y) across the cell.

Virtual microscope

Three-stage model

DIC microscope:

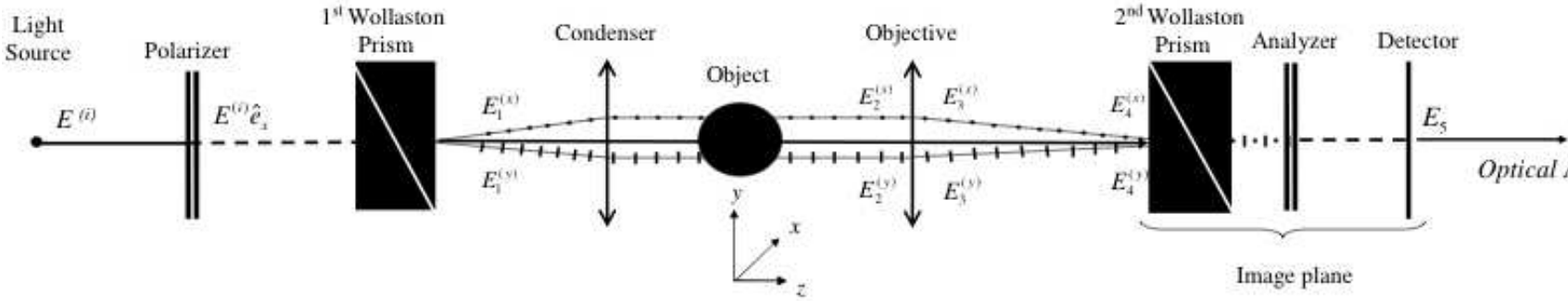

1. **Object → Objective** 2. **Objective** 3. **Objective → Detector**

Three-stage model

DIC microscope:

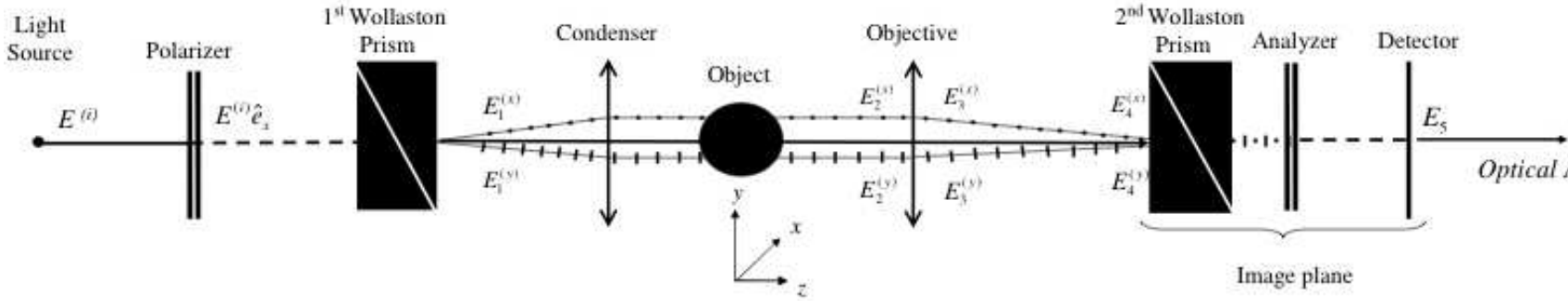

1. **Object → Objective** 2. **Objective** 3. **Objective → Detector**

Stage 1: Numerical solution of time-harmonic Maxwell's equations describing electromagnetic wave scattering by the cell:

$$i\omega\mathbf{B} + \nabla \times \mathbf{E} = 0, \qquad i\omega\mathbf{D} - \nabla \times \mathbf{H} = 0,$$

Three-stage model

DIC microscope:

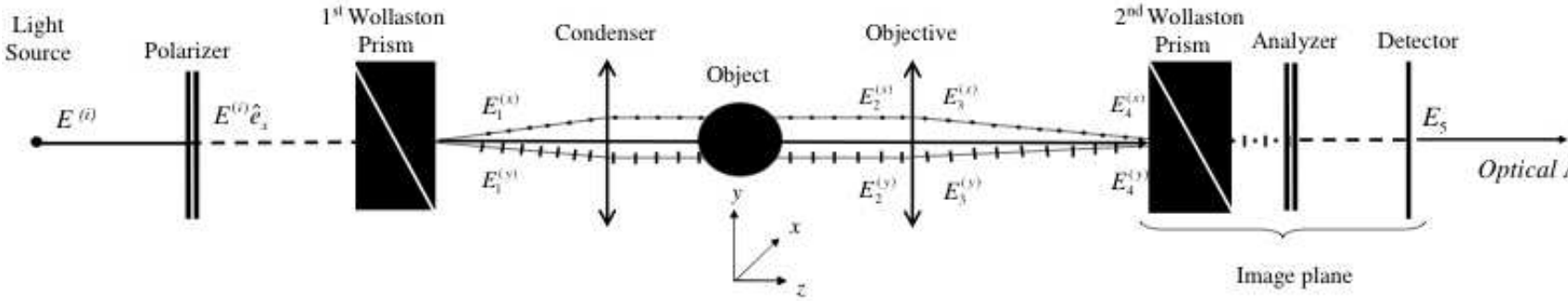

1. **Object → Objective** 2. **Objective** 3. **Objective → Detector**

Stage 1: Numerical solution of time-harmonic Maxwell's equations describing electromagnetic wave scattering by the cell:

$$i\omega\mathbf{B} + \nabla \times \mathbf{E} = 0, \qquad i\omega\mathbf{D} - \nabla \times \mathbf{H} = 0,$$

For isotropic media we can use the constitutive relations: $\mathbf{B} = \mu\mathbf{H}$ and $\mathbf{D} = \varepsilon\mathbf{E}$, where μ is a constant permeability and $\varepsilon = n^2$ is a space-dependent permittivity.

Objective Lens

Objective Lens

Stage 2: objective is modeled as a thin lens satisfying the geometrical optics lens law:

$$\frac{1}{f} = \frac{1}{z_1} + \frac{1}{z_i},$$

where f is a focal distance, z_1 is an object-to-lens and z_i is a lens-to-detector distances.

Fields on the exit pupil

The field components $U = \{E_x, E_y, E_z\}$ are computed according to *Goodman,* **Introduction to Fourier Optics**:

$$U_l^{'}(x, y) = T_l U_l(x, y)$$

Fields on the exit pupil

The field components $U = \{E_x, E_y, E_z\}$ are computed according to *Goodman,* **Introduction to Fourier Optics**:

$$U_l^{'}(x,y) = T_l U_l(x,y)$$

where

$$T_l = e^{\frac{-ik(x^2+y^2)}{2f}} \times \begin{cases} 1 & \text{inside the lens,} \\ 0 & \text{otherwise} \end{cases}$$

is a paraxial approximation of the phase transfer function multiplied by the pupil function

Fields on the exit pupil

The field components $U = \{E_x, E_y, E_z\}$ are computed according to *Goodman,* **Introduction to Fourier Optics**:

$$U_l^{'}(x,y) = T_l U_l(x,y)$$

where

$$T_l = e^{\frac{-ik(x^2+y^2)}{2f}} \times \begin{cases} 1 & \text{inside the lens,} \\ 0 & \text{otherwise} \end{cases}$$

is a paraxial approximation of the phase transfer function multiplied by the pupil function

The focusing error aberration effect on phase is given by multiplying T_l by $W_a(x,y) = exp\left[-\frac{ik(x^2+y^2)}{2}\left(\frac{1}{z_a} - \frac{1}{z_i}\right)\right]$, where $z_a \neq z_i$

Objective $\rightarrow$ Detector Plane

The fields components U projected on the detector plane using Fresnel integral:

$$U^d(\xi,\eta) = \frac{e^{ikz_i}}{i\lambda z_i} \iint_{-\infty}^{\infty} U_l'(x,y) e^{\frac{ik[(x-\xi)^2+(y-\eta)^2]}{2z_i}} dxdy$$

Objective → Detector Plane

The fields components U projected on the detector plane using Fresnel integral:

$$U^d(\xi,\eta) = \frac{e^{ikz_i}}{i\lambda z_i}\iint_{-\infty}^{\infty} U_l'(x,y)e^{\frac{ik[(x-\xi)^2+(y-\eta)^2]}{2z_i}}dxdy$$

The DIC effect on the detector plane is achieved by introducing shifted field interference:

$$I^2_{DIC} = |E_x^{TE}(x+\delta_s/2, y+\delta_s/2)|^2 + |E_y^{TE}(x+\delta_s/2, y+\delta_s/2)|^2 + |E_z^{TM}(x-\delta_s/2, y-\delta_s/2)|^2,$$

where δ_s is a shear distance and TE and TM correspond to the transverse electrical (perpendicular) and the transverse magnetic (parallel) polarization.

Experiments

Parameters

We simulate the image formation process of $82\mu m$ in diameter polystyrene sphere with the refraction index $n_{sphere} = 1.6$ immersed in water ($n = 1.33$) *in-* and *out-of-focus*.

Parameters

We simulate the image formation process of $82\mu m$ in diameter polystyrene sphere with the refraction index $n_{sphere} = 1.6$ immersed in water ($n = 1.33$) *in-* and *out-of-focus*.

The DIC microscope specifications are:

Aperture radius $\rho = 1.5mm$

Focal distance $f = 6.6mm$

The distance between the objective and the detector plane is $z_1 = 164.5mm$

Wavelength range $\lambda = [0.501 - 0.580]\mu m$

Model validation

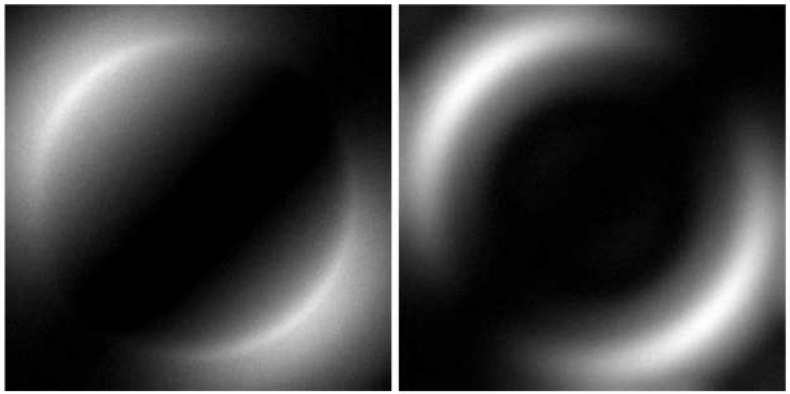

(a) (b)

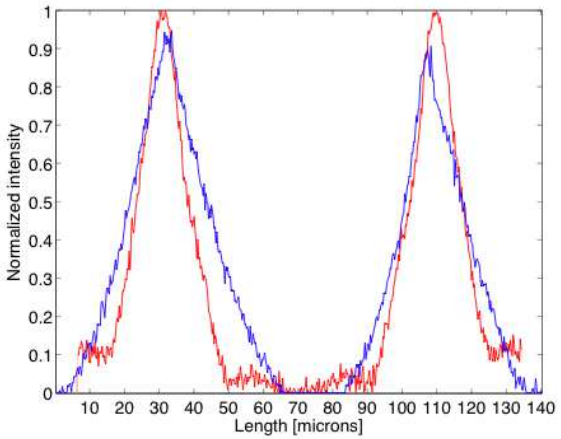

(c)

(a) recorded image of $82\mu m$ in polystyrene sphere taken $40\mu m$ above the focus;
(b) simulated image;
(c) diagonal profile of intensity of recorded (blue line) and simulated (red line) images.

Numerical methods

Scattering by the dielectric sphere

Mie series solution (TM mode):

$$E^i(k\vec{r}) = \sum_{n=1}^{\infty} E_n[M_{o1n}^{(1)} + iN_{e1n}^{(1)}]$$

$$E^{int}(mk\vec{r}) = \sum_{n=1}^{\infty} E_n[c_n M_{o1n}^{(1)} + id_n N_{e1n}^{(1)}]$$

$$E^s(k\vec{r}) = \sum_{n=1}^{\infty} E_n[ia_n N_{e1n}^{(3)} - M_{o1n}^{(3)}]$$

Scattering by the dielectric sphere

Mie series solution (TM mode):

$$E^i(k\vec{r}) = \sum_{n=1}^{\infty} E_n[M_{o1n}^{(1)} + iN_{e1n}^{(1)}]$$

$$E^{int}(mk\vec{r}) = \sum_{n=1}^{\infty} E_n[c_n M_{o1n}^{(1)} + id_n N_{e1n}^{(1)}]$$

$$E^s(k\vec{r}) = \sum_{n=1}^{\infty} E_n[ia_n N_{e1n}^{(3)} - M_{o1n}^{(3)}]$$

where a_n, b_n, c_n, d_n are the unknown scattered and internal field expansion coefficients computed from the condition $(E^i + E^s - E^{int}) \times \hat{e}_r = 0$

Scattering by the dielectric sphere

Mie series solution (TM mode):

$$E^i(k\vec{r}) = \sum_{n=1}^{\infty} E_n[M_{o1n}^{(1)} + iN_{e1n}^{(1)}]$$

$$E^{int}(mk\vec{r}) = \sum_{n=1}^{\infty} E_n[c_n M_{o1n}^{(1)} + id_n N_{e1n}^{(1)}]$$

$$E^s(k\vec{r}) = \sum_{n=1}^{\infty} E_n[ia_n N_{e1n}^{(3)} - M_{o1n}^{(3)}]$$

where a_n, b_n, c_n, d_n are the unknown scattered and internal field expansion coefficients computed from the condition $(E^i + E^s - E^{int}) \times \hat{e}_r = 0$

m is the ratio between n_o and n_m, $E_n = i^n \frac{2n+1}{n(n+1)}$,

Scattering by the dielectric sphere

Mie series solution (TM mode):

$$E^i(k\vec{r}) = \sum_{n=1}^{\infty} E_n[M_{o1n}^{(1)} + iN_{e1n}^{(1)}]$$

$$E^{int}(mk\vec{r}) = \sum_{n=1}^{\infty} E_n[c_n M_{o1n}^{(1)} + id_n N_{e1n}^{(1)}]$$

$$E^s(k\vec{r}) = \sum_{n=1}^{\infty} E_n[ia_n N_{e1n}^{(3)} - M_{o1n}^{(3)}]$$

where a_n, b_n, c_n, d_n are the unknown scattered and internal field expansion coefficients computed from the condition $(E^i + E^s - E^{int}) \times \hat{e}_r = 0$

m is the ratio between n_o and n_m, $E_n = i^n \frac{2n+1}{n(n+1)}$,

M_{o1n} and N_{e1n} are spherical harmonics computed using Legendre functions and spherical Bessel functions of 1st and 3rd kind.

Fresnel Integral

We approximate the double integral using the 1D points/weights distribution solving the following system:

$$\int_{-1}^{1} \omega(x) f(x) dx = \sum_{k=1}^{n} \omega_k f(x-k) + R_n(f)$$

where we choose weight function $\omega(x) = 1$, x_k are roots of Legendre polynomials.

Fresnel Integral

We approximate the double integral using the 1D points/weights distribution solving the following system:

$$\int_{-1}^{1} \omega(x) f(x) dx = \sum_{k=1}^{n} \omega_k f(x-k) + R_n(f)$$

where we choose weight function $\omega(x) = 1$, x_k are roots of Legendre polynomials.

The nodes x_k and the weights ω_k are derived via decomposition of Jacobi matrix associated with Legendre polynomial coefficients.

Fresnel Integral

We approximate the double integral using the 1D points/weights distribution solving the following system:

$$\int_{-1}^{1} \omega(x) f(x) dx = \sum_{k=1}^{n} \omega_k f(x-k) + R_n(f)$$

where we choose weight function $\omega(x) = 1$, x_k are roots of Legendre polynomials.

The nodes x_k and the weights ω_k are derived via decomposition of Jacobi matrix associated with Legendre polynomial coefficients.

$R_n(f)$ is the error of approximation (integration is exact for polynomials of degree $2n-1$).

Concluding remarks

Discussion and work in progress

The main goal of this project is to reconstruct refractive index distribution within the cell, use it to detect aneuploidy and answer the questions:

Discussion and work in progress

The main goal of this project is to reconstruct refractive index distribution within the cell, use it to detect aneuploidy and answer the questions:

- What are the bounds and limitations of using light as a biomarker?

Discussion and work in progress

The main goal of this project is to reconstruct refractive index distribution within the cell, use it to detect aneuploidy and answer the questions:

- What are the bounds and limitations of using light as a biomarker?
- What is a computational complexity of the approach? How could it be effectively parallelized?

Discussion and work in progress

The main goal of this project is to reconstruct refractive index distribution within the cell, use it to detect aneuploidy and answer the questions:

- What are the bounds and limitations of using light as a biomarker?
- What is a computational complexity of the approach? How could it be effectively parallelized?
- Would trust-region non-linear optimization methods be sufficient for reconstruction of refractive index distribution or we should use a probabilistic approach?

Discussion and work in progress

The main goal of this project is to reconstruct refractive index distribution within the cell, use it to detect aneuploidy and answer the questions:

- What are the bounds and limitations of using light as a biomarker?
- What is a computational complexity of the approach? How could it be effectively parallelized?
- Would trust-region non-linear optimization methods be sufficient for reconstruction of refractive index distribution or we should use a probabilistic approach?

Project Support:

- *Enterprise Ireland Commercialisation Fund* (funds feasibility study for application of this research to IVF).
- *Nvidia Corp.* (donated 2×2880 cores General Purpose GPU cluster).